SCIENCE CHINA
Earth Sciences

•ARTICLE•

https://doi.org/10.1007/s11430-023-1220-1

Potassium isotopic signatures of modern offshore detrital sediments from different climatic regimes and the implications

Jun MU[1], Tianyu CHEN[1], Qian YU[2], Shichao AN[1], Jianfang CHEN[3], Xuefa SHI[4] & Weiqiang LI[1*]

[1] *State Key Laboratory for Mineral Deposits Research, School of Earth Sciences and Engineering, Nanjing University, Nanjing 210023, China;*
[2] *Ministry of Education Key Laboratory for Coast and Island Development, School of Geography and Ocean Science, Nanjing University, Nanjing 210023, China;*
[3] *State Key Laboratory of Satellite Ocean Environment Dynamics, Second Institute of Oceanography, Ministry of Natural Resources, Hangzhou 310012, China;*
[4] *Key Laboratory of Marine Geology and Metallogeny, First Institute of Oceanography, Ministry of Natural Resources, Qingdao 266061, China*

Received March 16, 2023; revised October 10, 2023; accepted November 2, 2023; published online January 22, 2024

Abstract Potassium isotopes are a novel tracer for continental weathering. Previous K isotope studies on chemical weathering generally targeted weathering profiles under a particular climate region, yet the effects of chemical weathering on K isotopes under different climatic backgrounds remain unclear. Moreover, little is known about the K isotope signatures of modern unconsolidated detrital sediments. Here, we report K isotopic data of surficial seafloor sediments from continental shelves along the east coast of China (ECC), as well as those around the tropical Hainan island in the northern South China Sea. The ECC sediments have a relatively narrow distribution of δ^{41}K (with reference to NIST3141a) values, which range from (−0.40±0.01)‰ to (−0.57±0.04)‰, with an average of (−0.51±0.09)‰. By contrast, δ^{41}K values of Hainan offshore sediments display a larger variation, ranging from (−0.28±0.07)‰ to (−0.67±0.02)‰. The δ^{41}K values of Hainan offshore sediments exhibit negative correlations with the chemical index of alteration (CIA), Al/K, Ti/K, and total iron (Fe_T), which underlines the control of chemical weathering on K isotopic signatures of detritus inputs into oceans. We also measured Mg isotope compositions for the same samples; interestingly, the variability in δ^{26}Mg of the samples is small (~0.24‰) for all ECC and Hainan offshore sediments, and δ^{26}Mg values do not show clear correlations with indexes of chemical weathering. Our study demonstrates the link between K isotopic variability of detrital sediments and climatic conditions including rainfall intensity, which indicates that K isotopes of the detrital component of marine sediments could be applied to study Earth's climate in deep time. The δ^{41}K values of the offshore detrital sediments are significantly less variable than those of pelagic marine sediments, highlighting the importance of distinguishing the effects of diagenesis and neoformation of clay minerals from continental weathering in attempts to study deep-time climate-weathering link by K isotopes in detrital sedimentary records.

Keywords Potassium isotopes, Magnesium isotopes, Chemical weathering, Detrital sediments, Climatic regimes, Mean annual precipitation

Citation: Mu J, Chen T, Yu Q, An S, Chen J, Shi X, Li W. 2024. Potassium isotopic signatures of modern offshore detrital sediments from different climatic regimes and the implications. Science China Earth Sciences, 67, https://doi.org/10.1007/s11430-023-1220-1

* Corresponding author (email: liweiqiang@nju.edu.cn)

1. Introduction

Chemical weathering of silicates exerts a primary control on the atmospheric CO_2 budget, influencing Earth's climate over geological timescales; in turn, climatic difference has a significant impact on the dynamics and products of silicate weathering (Eberl, 1984; Kump et al., 2000; Beaulieu et al., 2010; Hu et al., 2014; Penman et al., 2020). Studies of the history of silicate weathering can improve our understanding of climate change at different time scales (Raymo and Ruddiman, 1992; Pogge von Strandmann et al., 2013; Sun et al., 2018). Chemical weathering is a critical process of global element cycling, through which elements and isotopes fractionate and distinct isotopic reservoirs formed over time (e.g., Penniston-Dorland et al., 2017; Teng, 2017; Wang et al., 2021a). Stable isotopes of metals are powerful tools to trace the various supergene geologic processes and to reconstruct the history of silicate weathering (e,g., Mg, Li, Zn, Cu, Moynier et al., 2017; Penniston-Dorland et al., 2017; Teng, 2017). For example, Mg isotopes fractionate significantly during silicate weathering (e.g., Teng et al., 2010; Huang et al., 2012; Liu et al., 2014; Ma et al., 2015), and Mg isotopes of detrital sediments have been applied to study deep-time weathering processes (e.g., Shen et al., 2009; Huang et al., 2016; Chen X Y et al., 2020). Another emerging system is stable K isotopes, which have also been shown to be sensitive to chemical weathering and biogeochemical cycles of K (Li S L et al., 2019; Wang et al., 2021a).

Most potassium in the Earth's crust is stored in silicate minerals, thus, the mass balance of K isotopes of siliciclastic sediments is not influenced by the carbonates. Significant variations of K isotope compositions have also been reported in plants and soils (Christensen et al., 2018; Li W S et al., 2021a, 2022b), riverine dissolved load (Li S L et al., 2019; Wang et al., 2021b; Li X Q et al., 2022), pore water (Santiago Ramos et al., 2018), marine sediments (Hu et al., 2020), and altered oceanic crust (Parendo et al., 2017; Liu et al., 2020; Santiago Ramos et al., 2020). Specifically, it has been shown that ^{39}K is preferentially retained in secondary clays during weathering of mafic and felsic igneous rocks, whereas ^{41}K is enriched in the fluid phases (Chen H et al., 2020; Teng et al., 2020; Li W S et al., 2021b). Therefore, K isotopes could also be used to trace the chemical weathering processes in geological time.

Isotopic fractionation of elements during silicate weathering is associated with decomposition of primary minerals and formation of secondary minerals, and the solid phase is complementary to the aqueous phase in terms of isotopic compositions (e.g., Santiago Ramos et al., 2018; Teng et al., 2020). The stable isotope ratios of several metals (i.e., Li, Mg, K) in river waters are sensitive to modern continental weathering processes (e.g., Dellinger et al., 2015; Li S L et al., 2019; Wang et al., 2021b), but isotopic signatures of river waters are transient and unlikely to be preserved in geologic records. By contrast, the sedimentary records could serve as the archive of continental weathering through the Earth's history. Terrigenous sediments hold 90% of continental K input to the ocean, yet our knowledge of the K isotopes in such sediments is limited. Hu et al., (2020) reported K isotopic compositions of deep ocean sediments from different localities, however, the sediments are pelagic and are mixtures of detrital, biogenic and authigenic components, which complicates the discussion on the K isotope signatures of terrigenous sediments in relation to silicate weathering. More recently, K isotope compositions of sediments from continental margins and ocean basins have been reported (Li W S et al., 2022a; Parendo et al., 2022b), and K isotope variabilities in weathering profiles of mafic and felsic rocks have been documented (Chen H et al., 2020; Teng et al., 2020). To date, the effects of chemical weathering on K isotopic compositions of weathered residues under different climatic regimes remain unclear.

In this study, we performed high-precision K isotope analyses on the surficial seafloor sediments of continental shelves along the east coast of China (ECC), including the Bohai Sea, Yellow Sea, East China Sea, as well as Hainan offshore of South China Sea. These unconsolidated sediments are fed by rivers and cover a wide range of climosequence, namely the temperate, subtropical, and tropical monsoon climatic regimes. The K isotope data of the shelf sediments provides an opportunity to better understand K isotope behaviors and the controlling factors during continental weathering under different climatic regimes. Our results confirm the sensitive response of K isotopes to intense chemical weathering, even in the detrital sedimentary record. This study reveals a potential link between K isotopes in detrital sediments and climatic conditions, which paves a way towards the application of K isotopes in sedimentary archives for investigating paleoclimate and paleocontinental weathering. Additionally, our study provides insights into the K isotope heterogeneity of the continental crust.

2. Geological setting and samples

As shown in Figure 1, the sampling sites are along China's east coast around three estuaries: the Yellow River, the Yangtze River, and the Minjiang River. The Yellow River is the second longest river in China, traveling through temperate-arid and semiarid climate zones with mean annual precipitation of 527 mm (http://www.ncdc.ac.cn). It carries 100 Mt/yr of sediments into the Bohai Sea in recent decades with an average water discharge of 1.45×10^{10} m^3/yr (Yu et al., 2013). The Yangtze River has water and sediment discharges of 8.96×10^{11} m^3/yr and 3.90×10^{8} tons/yr, respectively (Guo

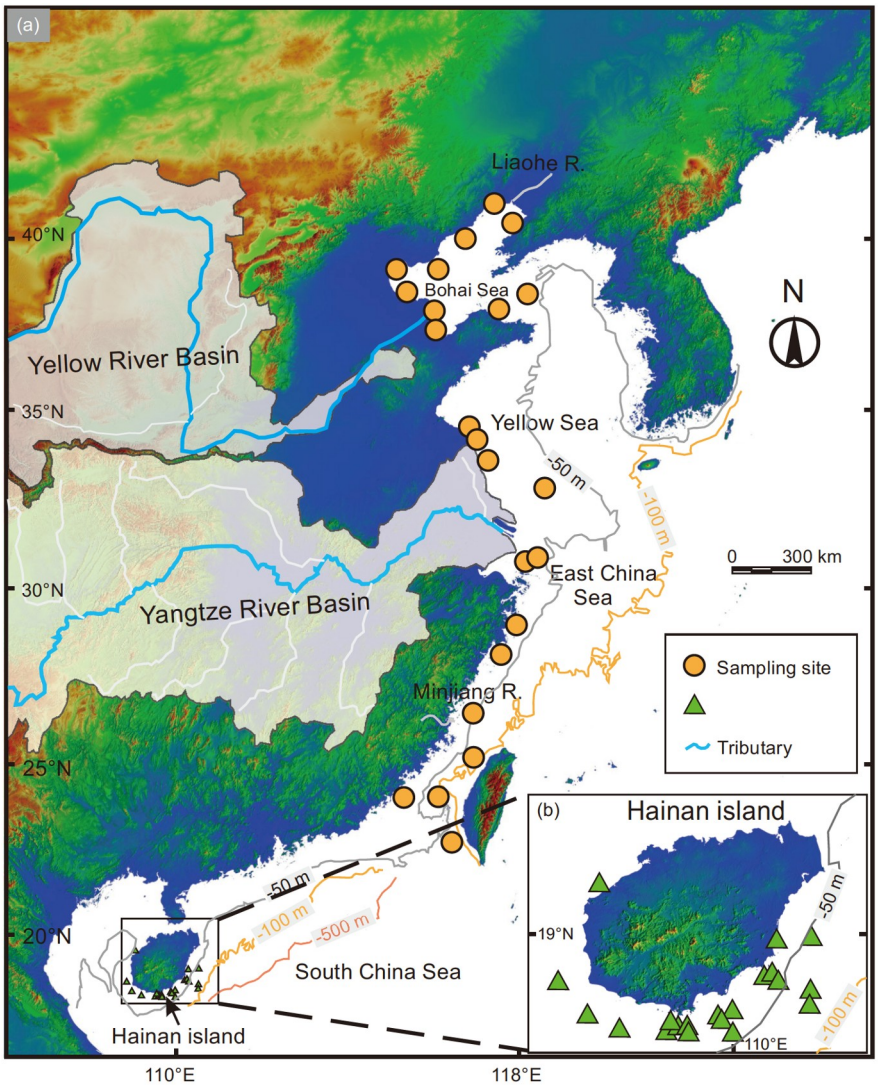

Figure 1 Sampling sites of shallow-sea shelf sediments on the east coast of China, including the Bohai Sea, the Yellow Sea, the East China Sea (a), and the Hainan island offshore (b).

and Yang, 2016). The Yangtze River catchment covers the whole subtropical monsoon climate zone, and its annual precipitation ranges from 859 to 1528 mm, averaging 1045 mm (Chen et al., 2014). Compared to the Yellow River and Yangtze River, the Minjiang River is a provincial-scale small river in southeast China with an annual mean runoff of 1760 m^3/s (Zhang et al., 2015).

These rivers delivered a huge amount of sediments to the ocean, and the complex hydrodynamic conditions led to the formation of different sediment types. The fine-grained mud is usually deposited at the river mouth regions (e.g., the Yellow River and Yangtze River) (Qiao et al., 2017). The sand deposits mainly occur at the outer shelf where the strong hydrodynamics (i.e., ocean currents, waves) prevail (Mi et al., 2022). Moreover, delta deposits characterized by sand, silt and clay mixture were also developed in the coastal area.

As for the Hainan offshore (Figure 1b), the samples were collected from the continental shelf near the tropical mountainous part of Hainan, where intense weathering is exemplified by the occurrence of laterite, bauxite, higher kaolinite, illite, and chlorite (Hu et al., 2014; Wei et al., 2021). The sediment source of Hainan offshore is characterized by the absence of alluvial plains, and the sediments are products of weathered bedrocks without multiple sediment recycling. The Hainan island has a higher annual temperature (22.8–25.8°C) and annual rainfall (960 mm to 2140 mm) relative to the east coast of China.

In this study, forty-three surficial seafloor sediments were obtained for K and Mg isotope analyses. All of the samples were from the upper 0–4 centimeters depths of settled sediments. Based on the rate of deposition, these detrital sediments were deposited within 20 yrs, and the possible early diagenesis to alter the terrestrial signals including K-Mg

isotopes registered in the detrital seafloor sediments would be minimal. The samples are from the ECC and Hainan offshore area, which span 22° in latitude (18°N to 40°N) and cover the region of temperate, subtropical, and tropical monsoon climatic regimes. Detailed information of the major and trace elements and neodymium isotopes of the samples are available in Wei et al. (2021).

3. Analytical methods

3.1 Sample treatment and ion exchange chromatography

After the removal of visible plant roots and shells by hand-picking under a stereo-microscope, approximately 50 mg of each bulk sediment sample was placed into a centrifuge tube and leached in 0.2 mol/L acetic acid for 36 hours to dissolve the carbonate and indistinguishable shells. The dissolved loads were decanted after centrifuging. Then the samples were washed in deionized water (18.2 MΩ/cm) and centrifuged. This procedure was repeated three times. Subsequently, the exchangeable cations in silicate minerals were liberated by 1 mol/L ammonium acetate at pH ≈ 7 for 48 hours. Identical to the leaching steps, the remaining solid was separated by centrifugation, followed by a triple wash with deionized water. Finally, the residue was transferred into a Teflon beaker for further digestion and purification.

Double-distilled concentrated hydrofluoric acid (HF), nitric acid (HNO_3), and hydrochloric acid (HCl) were used for sample digestion. Each sample was placed in a screw-top Teflon beaker and dissolved in 3 mL of mixed concentrated HF and HNO_3, which was heated on a hotplate at 130°C for 48 hours. For occasional incomplete sample digestion, the samples were evaporated to near dryness, then digested in a mixture of 3 mL concentrated HCl, 1 mL concentrated HNO_3 and 0.5 mL $HClO_4$ and heated at 150°C until the complete disappearance of the solid. After that, all the dissolved samples were dried and re-dissolved in 2 mL 2% HNO_3 (v/v). A 0.2 mL aliquot of the solution was taken and diluted into 3 mL 2% HNO_3 (v/v) for elemental analysis by ICP-OES. Based on the elemental analytical results, one aliquot of the sample solution that contained ~ 50 μg of K and Mg was transferred into a new beaker that dried at 95°C and re-dissolved three times in 0.1 mL concentrated HNO_3 to transform cations to nitrate form. Lastly, the sample was heated to dryness and dissolved in 500 μL of 1.5 mol/L HNO_3 prior to chemical purification.

Purification of K and Mg followed the well-established protocol detailed in Li et al. (2016). In brief, a two-stage column procedure was used, and 1 mL volume of 100–200 mesh BioRad® AG50W-×12 resin and 0.4 mL volume of 100–200 mesh BioRad® AG50W-×8 resin were packed in the first- and second-stage columns, respectively. Simultaneous separation of K and Mg from the matrix was achieved in the first stage, and then the two elements were separately collected in two cuts in the 2nd stage column. The two-stage column chemistry achieved recovery higher than 99% for both K and Mg. The total procedural blank of K and Mg were <10 and <20 ng, respectively, which are negligible compared to the mass (>50 μg) of the two elements in the samples. After column chemistry, the purified Mg and K were re-dissolved in 2% HNO_3 (v/v) for isotope analyses.

3.2 Potassium and magnesium isotope analysis

Potassium isotope analysis was performed on a Nu 1700 Sapphire High-Resolution Multi-Collector Inductively Coupled Plasma Mass Spectrometer (HR-MC-ICP-MS) housed at the State Key Laboratory for Mineral Deposits Research, Nanjing University, China, following the method described in detail by An et al. (2022). A brief description of the analytical method is given below. The instrument was running under a conventional dry and hot plasma setting with a standard 1300 W forward RF power. An Aridus III desolvating system was used for sample introduction. $^{40}ArH^+$ was resolved from $^{41}K^+$ by using high mass resolution (mass resolving power >16000) of the instrument, which provided interference-free shoulders of $^{41}K^+$ for isotopic measurement of $^{41}K/^{39}K$ ratios. Standard-sample bracketing (SSB) method was used to correct mass bias and instrumental drift, with each K sample bracketed by a 3 ppm (1 ppm=1 mg/L) in-house K isotope standard ("A-K", purchased from SPEX Company, USA). Based on repeat analyses of NIST SRM 3141a against the in-house A-K standard solution, the long-term external reproducibility of the K isotope analyses in this study is ±0.07‰ (n=20) for $^{41}K/^{39}K$.

Magnesium isotopes were measured on a Thermo Scientific Neptune Plus multi-collector mass spectrometer (MC-ICP-MS) at the State Key Laboratory for Mineral Deposits Research, Nanjing University, China. The detailed analytical method has been described by Liu and Li (2020). Standard-sample-standard bracketing was used during the analytical sessions to correct instrumental mass bias. Both potassium and magnesium isotope data are reported in delta notation relative to DSM3 for Mg isotopes and NIST 3141a for K isotopes, respectively, as defined below.

$$\delta^{26}Mg_{DSM3}(‰) = \left[\left(^{26}Mg/^{24}Mg\right)_{sample} / \left(^{26}Mg/^{24}Mg\right)_{DSM3} - 1\right] \times 1000, \quad (1)$$

$$\delta^{41}K_{NIST3141a}(‰) = \left[\left(^{41}K/^{39}K\right)_{sample} / \left(^{41}K/^{39}K\right)_{NIST3141a} - 1\right] \times 1000. \quad (2)$$

USGS rock standards AGV-2 and BHVO-2 were treated as unknown samples to validate the accuracy of the total chemical and mass spectrometry procedures. The K and Mg

isotope compositions of measured standards ($\delta^{41}K_{AGV\text{-}2}$=(−0.43±0.07)‰, $\delta^{26}Mg_{BHVO\text{-}2}$=(−0.19±0.07)‰) are consistent with the literature values within uncertainties (Teng, 2017; Wang et al., 2021a).

3.3 XRD analysis

The bulk-sediment mineral components analysis was performed on a Bruker D8 Advance Eco X-ray diffractometer instrument at State Key Laboratory for Mineral Deposit Research, Nanjing University. The bulk sediment samples were dried and handpicked under a stereo microscope to remove the visible plant and shell fragments. Then the samples were ground into powder (>200 mesh in grain size) for XRD analysis without additional leaching processes. The XRD instrument was running at 40 kV and 40 mA with a Cu Anode X-ray source. The XRD data processing and mineral identification were made using a Jade 6.5 software. The relative abundance of quartz, albite, orthoclase and clay minerals were estimated based on the area of characteristic diffraction peak intensity (i.e., (024) for quartz, (002) for albite, (-202) for orthoclase).

3.4 Grain size analysis

Approximately 2–5 grams of sediments were placed into small beakers and soaked in the dispersant—sodium hexametaphosphate ($Na(PO_4)_6$) with a concentration of 0.5% for 24 hours. Then, the grain-size distribution analysis was performed on the Mastersizer 2000 laser grain size analyzer (for the range 0.01–2000 μm), School of Geographic and Oceanographic Science, Nanjing University (Ma et al., 2010).

4. Results

4.1 Isotope results

The K-Mg isotope data of the bulk sediment samples are plotted in Figure 2 and tabulated in Table 1. The K isotopes in the detrital sediments from the east coast of China (ECC) are mildly fractionated, with $\delta^{41}K$ varying from (−0.40±0.01)‰ to (−0.57±0.04)‰, averaging at (−0.51±0.09)‰. The $\delta^{41}K$ values of ECC samples are lower than that of the bulk silicate earth (BSE), without a clear trend shown versus their latitudes (Figure 2b). The $\delta^{26}Mg$ values of the ECC samples vary from (−0.29±0.01)‰ to (−0.05±0.01)‰, which are higher than that of the mantle range (Figure 2c). Similarly, no clear trend is observed between $\delta^{26}Mg$ and latitude (Figure 2d). The sediments from offshore of the Hainan island have $\delta^{41}K$ values that range from (−0.28±0.07)‰ to (−0.67±0.02)‰, with an average of (−0.51±0.22)‰. The $\delta^{26}Mg$ values range from (−0.31±0.08)‰ to (0.08±0.03)‰, which is comparable to that of the ECC sediments. In short, there are ~0.4‰ and ~0.24‰ variations for the $\delta^{41}K$ and $\delta^{26}Mg$ values within the surficial seafloor sediments, respectively. Marine sediment samples from the Lower latitudes (Hainan island) display greater dispersion in $\delta^{41}K$ values than the mid-latitude regions (the Bohai Sea, the Yellow Sea, and the East China Sea).

4.2 Mineralogy of the sediment

Quartz, albite, orthoclase, calcite and halite are the main minerals in the bulk sediments as identified by powder XRD analysis (see supplementary data, https://link.springer.com). In addition, clay minerals, such as vermiculite, chlorite/kaolinite, and mica/illite, are identified based on XRD peaks with d-values of 14.4, 7.1, and 10 Å, respectively.

5. Discussion

5.1 Possible effects of diagenesis and clay authigenesis

Shallow-sea shelf sediments are characterized by terrigenous clastic sediments delivered by rivers from a wide range of sources. For example, the Bohai Sea, Yellow Sea and East China Sea in the mid-latitude region mainly receive detrital materials from the Yellow River, Huaihe River, and Yangtze River, respectively (Liu et al., 2018; Lu et al., 2019), and the sediments in the east-south coastal area of Hainan island are mainly derived from island rock denudation processes (Hu et al., 2014; Wei et al., 2021). These unconsolidated shallow seafloor sediments are unlikely to suffer from strong diagenesis without compaction and consolidation. This is also evidenced by the relations between Al, Sc, and Ti that are different from those of the authigenic clay (Figure 3). A group of clay minerals (i.e., kaolinite, smectite, chlorite, illite) in unconsolidated marine sediments were commonly regarded as an indicator for tracing the provenance of the sediments in China coast (e.g., Hu et al., 2014; Wang et al., 2015). Thus, the silicate components provide unbiased information about climate-related continental weathering on large-scale terrains (Dong et al., 2020; Wei et al., 2021).

Signatures of conservative trace elements (La-Th-Sc, Ti/Zr) and ε_{Nd} values indicate that the sources of these sediments have an average composition comparable to granite and granodiorite (Wei et al., 2021). The contents of Sc and Ti measured in the shelf sediments and their relationships with Al content have been utilized to indicate the contribution from authigenic clays to shelf sediments, because these trace elements are relatively depleted (Ti) or enriched (Sc) in the marine authigenic clays with long seawater exposure time (cf. Dunlea et al., 2015; Wei et al., 2020). For example, Ti in authigenic clays is relatively lower than that of the detritus, given the extremely low content of Ti in seawater (Wei et al.,

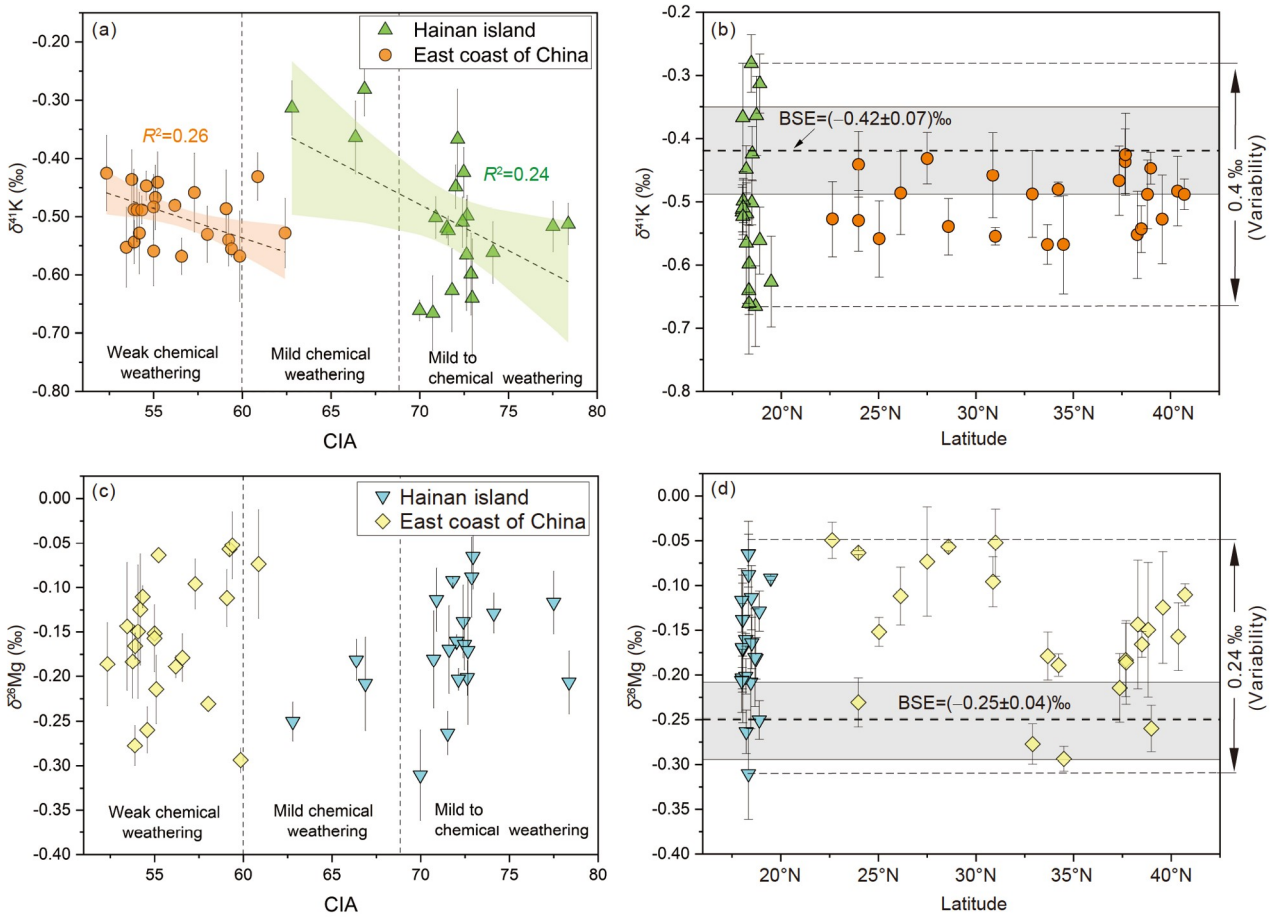

Figure 2 K-Mg isotopic compositions of the shallow-sea shelf sediments as a function of CIA and the latitude. (a) δ^{41}K values of sediments versus CIA. The linear fittings are shown with 95% confidence intervals. (b) δ^{41}K values of sediments versus the latitude. (c) δ^{26}Mg values of sediments versus CIA. (d) δ^{26}Mg values of sediments versus latitude. The CIA was calculated as $Al_2O_3/(Al_2O_3+CaO^*+Na_2O+K_2O)\times100$, where the content of CaO* is solely from silicate (Nesbitt and Young, 1982). The CIA values of the sediments are from Wei et al. (2021).

2020). Instead, Sc is relatively enriched in the pelagic authigenic clays due to hydrothermal inputs into oceans (Dunlea et al., 2015). In Figure 3, we compare the data of our samples with those of the upper continental crust (Rudnick and Gao, 2014) and modern marine authigenic clays from the South Pacific Gyre (Dunlea et al., 2015). The distinct element distribution fields and linear correlations between Al, Sc, and Ti confirm that the terrigenous sediments are essentially free of authigenic clay minerals (Figure 3). Glauconite was considered as a K sink and could elevate the δ^{41}K values of marine sediments (Li W S et al., 2022a), but it is not identified in our XRD analysis (see supplementary data). Therefore, the authigenic components are considered to be negligible in offshore sediments, which otherwise affects the interpretation of K isotopes in this study.

5.2 Mechanisms of K-Mg isotope fractionation in the shallow-sea shelf sediments

In this study, careful pretreatments (i.e., leaching by acetic acid and ammonium acetate) precluded the potential effects of exchangeable cations and carbonates on the K and Mg isotope compositions of the bulk sample. Other factors that potentially affect the distribution of K and Mg and their isotopes in the continental shelf sediments include (1) the degree of chemical weathering in the source regions; and (2) the transport and sorting history. The two factors are discussed separately below.

5.2.1 Chemical weathering control on the K isotopic variation of sediments

Continental weathering generally results in lower δ^{41}K and higher δ^{26}Mg values in the residual solid phase (e.g., Teng, 2017; Li S L et al., 2019; Chen H et al., 2020; Teng et al., 2020). The source regions of our samples cover temperate, subtropical, and tropical monsoon climatic regimes with a span of 22° in latitude. Previous studies have shown that the weathering intensity of river basins increases southwards (i.e., Liaohe River, Yellow River, Yangtze River, Minjiang River in order), and so does the formation of clay minerals

Table 1 Potassium and magnesium isotope compositions of modern offshore detrital sediments[a)]

Sample	CIA	K (%)	Al/K	Fe_T (%)	$\delta^{26}Mg$ (‰)	2SD	*N*	$\delta^{41}K$ (‰)	2SD	*N*	95% c.i. (‰)	Dominant grain size (μm)
BHS-1	54.3	2.19	3.3	3.63	−0.11	0.01	3	−0.49	0.03	4	0.02	11.90
BHS-2	54.2	2.33	3.3	4.43	−0.12	0.06	4	−0.53	0.09	4	0.07	6.40
BHS-3	54.1	2.15	3.2	3.84	−0.15	0.08	4	−0.49	0.07	4	0.05	7.30
BHS-4	54.6	2.06	3.2	3.77	−0.26	0.03	2	−0.45	0.03	4	0.03	9.30
BHS-5	53.5	2.2	3.1	3.56	−0.14	0.07	4	−0.55	0.09	4	0.07	13.40
BHS-6	53.9	1.71	3.1	3.2	−0.17	0.01	2	−0.54	0.09	8	0.04	8.20
BHS-7	52.3	2.01	3.2	3.54	−0.19	0.05	4	−0.43	0.08	4	0.06	13.40
BHS-8	53.8	1.82	3.2	3.24	−0.18	0.04	4	−0.44	0.06	4	0.05	17.10
BHS-9	55.1	1.86	3.3	3.53	−0.21	0.04	2	−0.47	0.07	4	0.06	31.50
ECS-1	62.4	1.54	3.3	2.63	−0.05	0.02	4	−0.53	0.14	8	0.06	5.70
ECS-2	58.0	1.27	4.1	3.14	−0.23	0.03	4	−0.53	0.06	4	0.05	
ECS-3	55.0	1.71	3.7	3.68	−0.15	0.02	3	−0.56	0.14	8	0.06	
ECS-4	59.4	2.44	3.4	5.09	−0.05	0.04	2	−0.55	0.02	4	0.01	7.30
ECS-5	57.3	1.99	3.4	4.14	−0.10	0.03	2	−0.46	0.09	4	0.07	8.20
ECS-6	59.1	2.13	3.4	4.28	−0.11	0.03	3	−0.49	0.08	4	0.07	
ECS-7	59.2	2.18	3.6	4.79	−0.06	0.00	2	−0.54	0.06	4	0.04	9.30
ECS-8	60.9	2.06	3.6	4.4	−0.07	0.06	4	−0.43	0.05	4	0.04	
ECS-9	55.2	1.66	2.6	2.12	−0.06	0.00	2	−0.44	0.12	8	0.05	
YS-1	55.0	2.27	3.1	3.46	−0.16	0.04	3	−0.48	0.07	4	0.06	8.20
YS-2	56.2	1.96	3.3	3.8	−0.19	0.01	2	−0.48	0.01	4	0.01	7.30
YS-3	59.9	2.18	3.3	4.66	−0.29	0.01	3	−0.57	0.12	5	0.08	35.60
YS-4	53.9	1.95	3.2	3.72	−0.28	0.02	4	−0.49	0.09	4	0.07	19.30
YS-5	56.6	1.92	3.4	3.85	−0.18	0.03	2	−0.57	0.04	4	0.03	19.30
HN-1	77.5	1.93	4.4	4.71	−0.12	0.04	2	−0.52	0.05	4	0.04	
HN-2	72.0	1.47	3.3	2.72	−0.16	0.01	2	−0.45	0.09	8	0.04	
HN-3	78.4	1.58	4.6	4.31	−0.21	0.04	3	−0.51	0.04	4	0.04	
HN-4	72.6	1.9	3.4	2.79	−0.20	0.02	4	−0.57	0.15	5	0.10	
HN-5	71.8	0.58	3.5	0.95	−0.09	0.00	2	−0.63	0.15	7	0.07	
HN-7	73.0	2.32	3.7	5.35	−0.07	0.04	2	−0.64	0.08	3	0.10	
HN-8	71.5	1.5	3.5	3.71	−0.26	0.02	3	−0.52	0.02	4	0.02	
HN-9	70.7	1.83	3.5	3.94	−0.18	0.05	3	−0.67	0.15	8	0.06	
HN-10	66.4	1.51	2.7	1.64	−0.18	0.02	2	−0.36	0.15	8	0.06	
HN-11	62.8	1.09	3.0	1.19	−0.25	0.02	3	−0.31	0.11	8	0.05	
HN-12	72.5	1.3	4.1	3.33	−0.16	0.03	3	−0.42	0.09	7	0.04	
HN-13	72.1	1.6	3.5	3.71	−0.20	0.01	2	−0.37	0.14	5	0.09	
HN-14	70.9	2.12	2.9	2.78	−0.11	0.04	2	−0.50	0.04	4	0.04	
HN-15	72.7	1.97	3.8	3.88	−0.17	0.08	2	−0.50	0.07	6	0.04	
HN-16	72.4	1.11	3.5	1.89	−0.14	0.04	4	−0.51	0.07	5	0.04	
HN-17	71.6	3.41	3.6	4.71	−0.17	0.05	3	−0.52	0.03	4	0.02	
HN-18	70.0	1.59	3.6	4.39	−0.31	0.05	3	−0.66	0.04	7	0.02	
HN-19	72.9	2.25	4.3	4.64	−0.09	0.05	2	−0.60	0.09	4	0.07	
HN-20	66.9	2.21	2.5	2.45	−0.21	0.05	4	−0.28	0.07	5	0.05	
HN-21	74.1	1.64	4.9	4.03	−0.13	0.02	2	−0.56	0.09	5	0.05	

a) CIA=$Al_2O_3/(Al_2O_3+CaO^*+Na_2O+K_2O)\times100$, where the content of CaO* is solely from silicate. Major element concentrations and CIA data are from Wei et al. (2021). 95% c.i.= 95% confidence interval calculated from 2SD with the student's factor. "*N*" represents the number of repeat analysis.

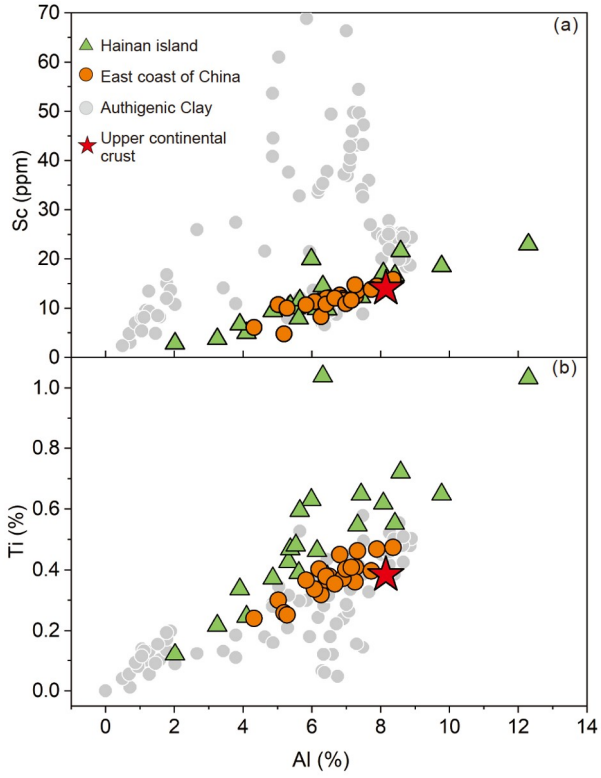

Figure 3 Cross plots of (a) Sc vs. Al, (b) Ti vs. Al of the bulk samples from the ECC and Hainan island offshore. The data of authigenic clays are from Dunlea et al. (2015). The data of the upper continental crust (UCC) are from Rudnick and Gao (2014).

(e.g., illite) (Li S L et al., 2019 and references therein). We use multiple weathering proxies, including the chemical index of alteration (CIA), Al/K, K/Ti, and Total iron (Fe_T), to evaluate this potential effect.

The shallow-sea shelf sediments from the ECC displayed low CIA values (52–62), with no significant variation in $\delta^{41}K$ values (Figure 2a), indicating relatively weak chemical weathering in the source regions. By contrast, The sediments from Hainan offshore exhibit higher CIA values (up to 79) and a remarkably greater variation in $\delta^{41}K$ values. The negative correlation between $\delta^{41}K$ and CIA in Hainan offshore sediments (Figure 2a) supports the previous finding that leaching of K is concomitant with preferential release of ^{41}K from primary silicate minerals (e.g., Li S L et al., 2019; Chen H et al., 2020; Teng et al., 2020; Li W S et al., 2021b). In addition, the correlations between $\delta^{41}K$ values and Al/K, K/Ti in Hainan offshore sediments confirm an apparent or possible control of chemical weathering of the source on the K isotope composition of the sediments (Figure 4a, 4b). The negative correlation between $\delta^{41}K$ and Fe_T (total of iron) (Figure 4c) is also supportive of chemical weathering control on K isotopes, because enhanced chemical weathering leads to the enrichment of Fe-bearing phases in the sediments (Wei et al., 2021). It is noteworthy that two samples are Krich with higher $\delta^{41}K$ values relative to the BSE value (Figure 2; Figure 4), and this might be related to source rock heterogeneity, such as alteration or K metasomatism that led to an elevation in both K content and $\delta^{41}K$ values in the source rock (e.g., Huang et al., 2020; Li W Q et al., 2020; Parendo et al., 2022a) before weathering and transportation to the coastal region. Similar phenomena of high K content (2.5–8.4 wt.%) with heavy K isotope data (up to −0.09‰) have been reported in the igneous and sedimentary rocks (Huang et al., 2020).

The $\delta^{26}Mg$ values of Hainan offshore sediments display a weak correlation with CIA, implying that the fractionation of Mg isotopes is also controlled by chemical weathering (Figure 2c). However, the variation of $\delta^{26}Mg$ in ECC sediments ((−0.29±0.01)‰ to (−0.05±0.01)‰) is comparable to that of the Hainan offshore ((−0.31±0.08)‰ to (0.08 ±0.03)‰) sediments and the $\delta^{26}Mg$ values exhibit no clear correlations with chemical weathering index Fe_T (Figure 4d), suggesting that Mg isotopes fractionation is associated with more complex processes relative to K isotopes. The cause of this comparable variation in $\delta^{26}Mg$ values of ECC and Hainan offshore sediments is likely related to the formation of complex Mg-bearing clay minerals during silicate weathering. The incipient and advanced weathering of primary minerals would fractionate Mg isotopes to different degrees, and a large variation of $\delta^{26}Mg$ in different clays (−1.85‰ to −0.18‰) has been documented in literature (Teng et al., 2010; Huang et al., 2012; Liu et al., 2014; Opfergelt et al., 2014; Ma et al., 2015; Li M Y H et al., 2021). Secondly, even for the same clay (e.g., vermiculite), Mg isotopes could exhibit different directions of fractionation during chemical weathering (Li M Y H et al., 2021). By contrast, K isotopes fractionate more significantly (~0.4‰ in $\delta^{41}K$ versus 0.24‰ in $\delta^{26}Mg$) and show a higher correlation with the chemical weathering proxies. In this regard, K isotopic fractionation seems less affected by the transformation of clay minerals relative to Mg isotopes during chemical weathering processes.

5.2.2 *Transport and sorting effects*

Sorting of sediments occurs during transportation in water, which could result in mineralogical and chemical differences between fine- and coarse-grained fractions (e.g., Huang et al., 2013; Hu et al., 2017). TiO_2/Zr is commonly used to trace the sediment sorting processes as Ti and Zr are preferentially retained in fine- and coarse-grained sediments, respectively (Garcia et al., 1994; Hu et al., 2017). Our results show that $\delta^{26}Mg$ values are weakly correlated to TiO_2/Zr ratios (Figure 5a) and the size of dominant fraction of sediments from the ECC (Figure 5b, also see the supplementary data), consistent with the observation that fine-grained clays enrich heavy Mg isotope (e.g., Hu et al., 2017). Yet, there is no clear correlation between $\delta^{41}K$ values and TiO_2/Zr ratios (Figure 5c)

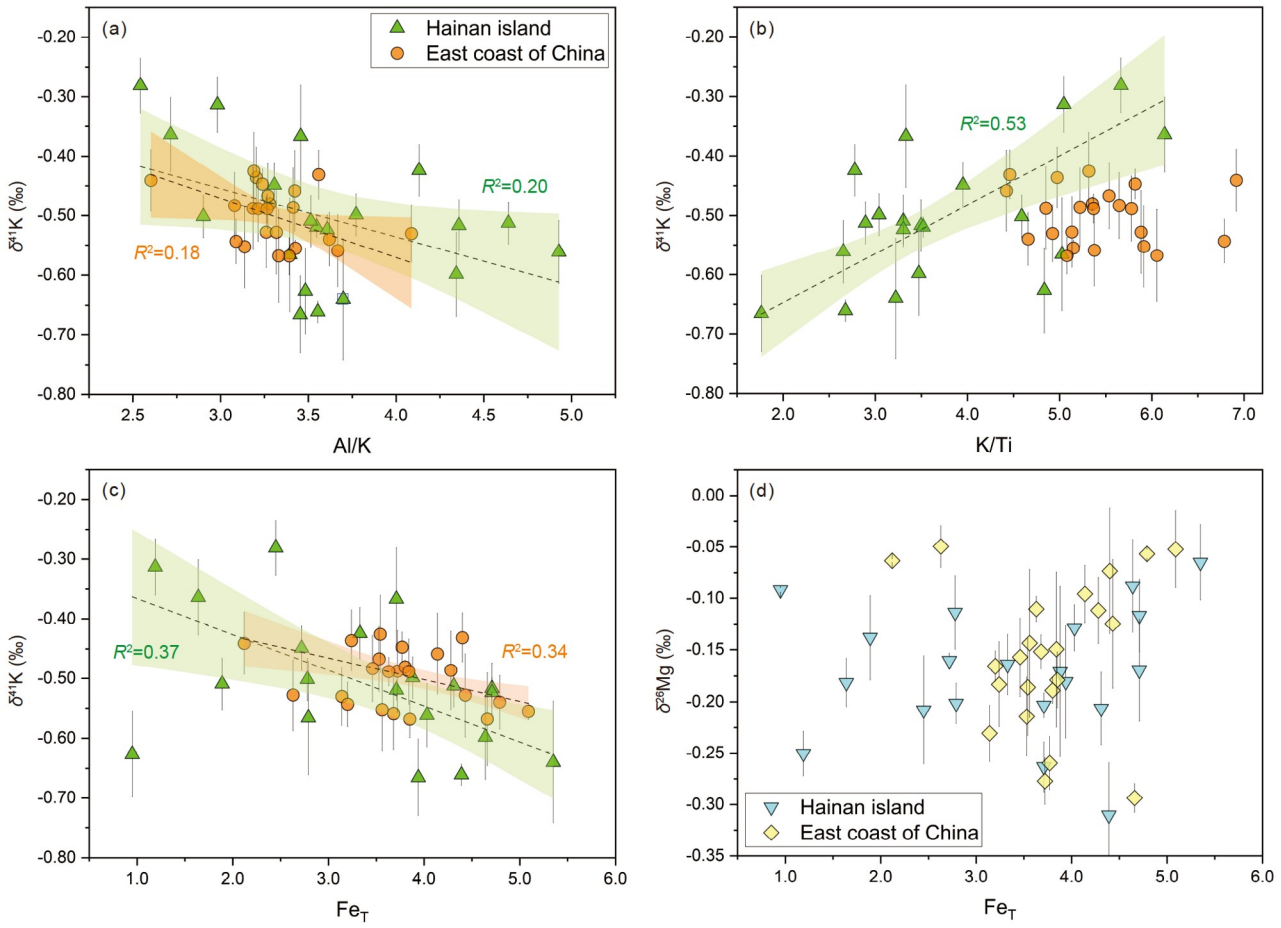

Figure 4 K-Mg isotopic variation versus chemical weathering proxies. (a) δ^{41}K vs. Al/K; (b) δ^{41}K vs. K/Ti; (c) δ^{41}K vs. Fe_T; (d) δ^{26}Mg vs. Fe_T. The linear fittings are shown with 95% confidence intervals.

and the size of dominant fraction of ECC samples (Figure 5d). As the fine fraction of sediments tend to have lower δ^{41}K values (Li S L et al., 2019), we speculate that the sorting effect on K isotopes could be masked by well mixing of weathered K-bearing minerals in the sediments due to complex transport dynamics of the sediments along the ECC.

Previous studies have pointed out that the seasonally varying hydrodynamic conditions were the major factors in controlling the sediments transport in the Bohai Sea, Yellow Sea, and East China Sea (Guan, 1994; Gao et al., 2016; Pang et al., 2016). Specifically, the settled surficial sediments were readily re-suspended and re-transported by the storms, tidal currents, and coastal currents, contributing to the well mixing of K-bearing primary and secondary minerals at a shallow surface. The relative homogeneity of the sediments is also demonstrated by the tight range of ratios of K/Ti and Al/K. Thus, we propose that the compositional uniformity of sediments could be responsible for the clustering K isotope data in the ECC sediments, as the post-depositional perturbation from the seasonal coastal ocean currents prevailed. Another reason may be the averaging effect of siliciclastic sediments from large rivers that drain various kinds of source rocks. This argument remains to be tested by future size-fraction-related K isotope studies. By contrast, the Hainan offshore is featured by seasonal variation of wind-driven tidal currents and the upwelling of seawater, with hydrodynamic conditions much weaker than the prevailing coastal currents in ECC (Chen et al., 2012; Hu and Wang, 2016; Li M et al., 2022). The Hainan offshore sediments are thus less likely to be intensely mixed after being transported to estuaries, which explains the greater variability in the δ^{41}K, as well as various chemical weathering indexes.

5.3 The potential link between climate and δ^{41}K of detrital sediments

The enhanced chemical weathering and the more scattered δ^{41}K values of the Hainan offshore sediments are correlated with their sediment sources' low latitude, high mean annual precipitation and temperature (MAP and MAT). Chemical weathering is enhanced under a warmer climate (i.e., higher runoff and temperature could facilitate the primary silicate minerals dissolution) (Dessert et al., 2001; Gaillardet et al., 2003), which could lead to greater fractionation of K iso-

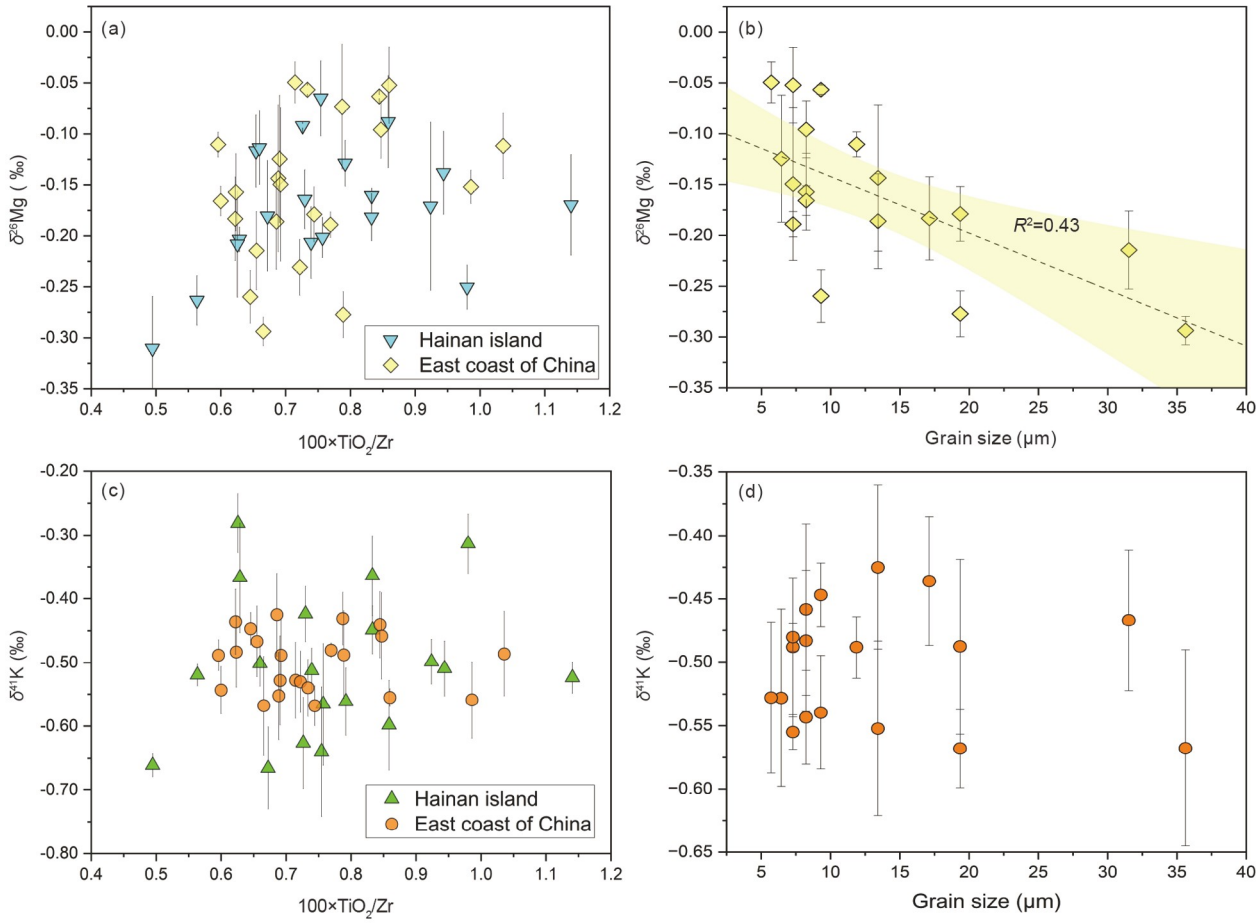

Figure 5 K-Mg isotope variation related to grain-size sorting during the transport of sediments. (a) δ^{26}Mg vs. TiO_2/Zr; (b) δ^{26}Mg versus the dominant size fraction of the sediments from the ECC; (c) δ^{41}K vs. TiO_2/Zr; (d). δ^{41}K versus the dominant size fraction of the sediments from the ECC. The linear fitting is shown with a 95% confidence interval.

topes.

To explore the potential relationship between K isotope fractionation and climate during continental weathering, we compiled the published K isotope compositions of weathered products of silicates and their regional MAP and MAT, as well as the K isotope data of this study and the corresponding MAP(T) for the samples source regions. The δ^{41}K values of the weathering residues display a rough decreasing trend as MAP increases (Figure 6a). By contrast, there is no clear relationship between MAT and δ^{41}K (Figure 6b). The decreasing trend between δ^{41}K values and MAP is also mirrored by the enhanced depletion of K content at higher MAP (Figure 6c). Rainfall facilitates the dissolution of primary minerals, leaching the water-soluble elements, leading to clay formation in solid residues (e.g., Muhs et al., 2001; Hayes et al., 2020). Long-term heavy rainfall advances the leaching stage for silicates, which may drive the regolith to a lower δ^{41}K value (e.g., Chen H et al., 2020; Teng et al., 2020). MAP control of δ^{41}K of weathering residues explains the comparable K isotope data between ECC sediments (−0.40‰ to −0.57‰) and those from the Mun River in Thailand (−0.41‰ to −0.60‰) (Li X Q et al., 2022), as the Yangtze and the Mun River basins have distinct MAT but similar MAP.

One could question whether modern MAP is representative of the all-time-averaged rainfall over the whole soil-development history. Although this is a concern, we argue that Earth's surface could be viewed as a steady system on certain time scales (Anderson, 2012), and the geographic setting is the primary control of MAP variation between different localities. The regolith (soil) residence time generally varies from 10^2 to 10^5 yrs (von Blanckenburg, 2006; Brantley, 2008; Sweeney et al., 2012). The rainfall reconstructed by simulation work and natural archives (i.e., lake sediments, cave deposits) shows that monsoon intensity periodically fluctuated and has not changed much in the past few ten to hundred millennia (Kutzbach et al., 2008; Chen et al., 2015; Cheng et al., 2016; Zhou et al., 2022). The top part of the regolith usually undergoes stronger leaching process, which could be imprinted by the lowest δ^{41}K signature. The relationship between δ^{41}K of weathered residue and MAP is a preliminary summary of

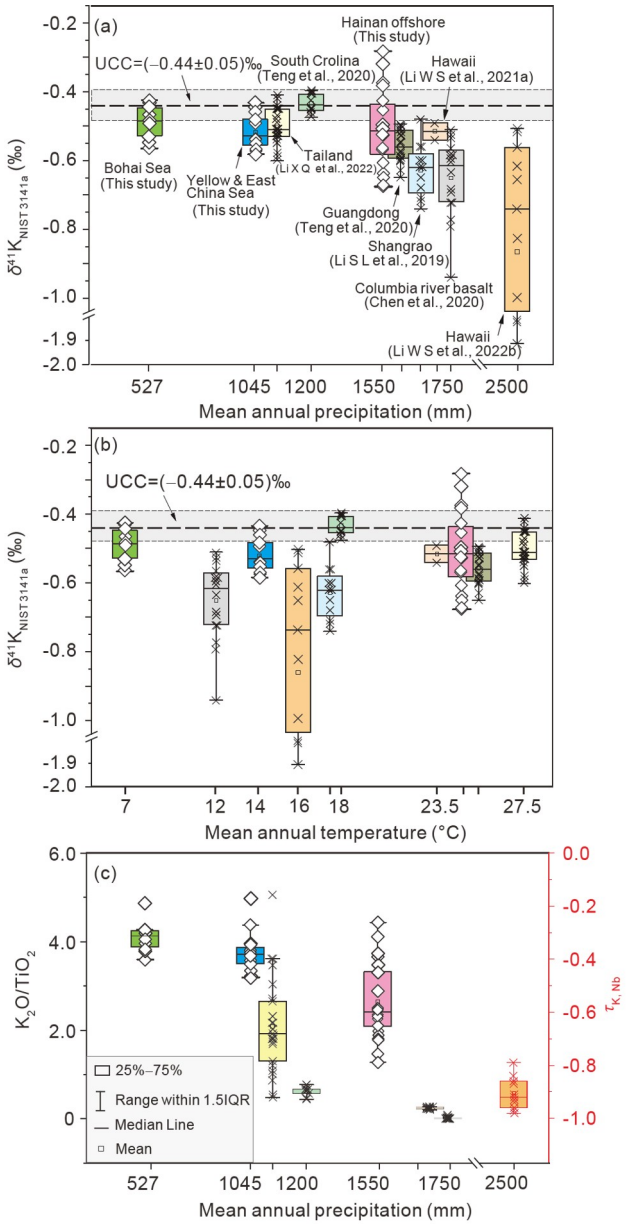

Figure 6 Compilation of K isotope data of weathered products and their relationships with mean annual precipitation and temperature. (a) δ^{41}K values of weathered products versus the mean annual precipitation (MAP) of their source region; (b) δ^{41}K values of weathered products versus mean annual temperature (MAT); (c) K_2O/TiO_2 ratios or $\tau_{K,Nb}$ value of the weathered products versus MAP. The MAP for sediments from the Bohai Sea is from the whole Yellow River basin (http://www.ncdc.ac.cn); the MAP for the Yellow and East China Sea are from the Yangtze River basin that provided detrital materials (Chen et al., 2014). The major elements contents, K isotope data and the corresponding MAP for Hawaii soil were from Li W S et al. (2021a, 2022b), river suspended load (Li S L et al., 2019; Li X Q et al., 2022) and weathering profiles (Chen H et al., 2020; Teng et al., 2020). Note that soil K isotope data were only collected from 20 to 150 kyr sites where chemical weathering dominated the section. The δ^{41}K value of upper continental crust (UCC) was from Huang et al. (2020). $\tau_{K,Nb}=(C_{K,w}\times C_{Nb,p})/(C_{K,p}\times C_{Nb,w})-1$, where C is the concentration of an element of interest, w and p are weathered, and parent materials, respectively (Kurtz et al., 2000). IQR, Interquartile range.

the present observations, and we welcome more follow-up studies to investigate this topic.

6. Implications

This study has great implications for the K isotope heterogeneity of the continental crust and the paleoclimate tracing. The K flux in the river sediments accounts for ~90% of the total riverine input of K into oceans (Viers et al., 2009). Most of the sediments fed by rivers were deposited on the continental shelf or back-arc basin in tectonic term with thousands of meters in thickness (Bian et al., 2010; Gao et al., 2016; Gong et al., 2016). On a time scale of Wilson cycles, partial melting of such near-shore sediments in back-arc basins (e.g., the modern western Pacific) could produce the source magma of S-type granites (Collins and Richards, 2008; Hopkinson et al., 2017; Xu et al., 2021). Hence, the large variation of δ^{41}K (−0.3‰ to −0.7‰) observed in the detrital sediments (Figure 7a, 7b) may provide new insight into the heterogeneous K isotope compositions of the igneous rocks (Figure 7c) in the continental crust.

Sedimentary rocks are common archives for the reconstruction of environmental and climatic changes. Identifying the effects of diagenesis and clay neoformation on those marine sedimentary records is of great significance to study deep-time climatic events by K isotopes, since the marine sediments that experience diagenesis and pelagic sediments are much more variable in K isotope compositions than those of detrital sediments (e.g., Hu et al., 2020; Li W S et al., 2022a). The post-depositional diagenetic alteration may also blur the continental weathering signals in the marine sedimentary records. In this study, we investigated the relationship between K isotopes in modern marine detritus and climatic conditions. We found that the mild-to-intense continental weathering could result in significant K isotope variability in terrigenous marine sediments. Moreover, an apparently negative correlation is seen while the MAP exceeds 1550 mm. These findings hint at the potential of K isotopes in sedimentary rocks for investigating paleoclimate and chemical weathering intensity in geologic history. Because K isotope ratios of weathering products are sensitive to chemical weathering and high MAP is associated with decreasing δ^{41}K values of weathered residues, the K isotopes may be a useful tool for studying deep-time extreme climatic events.

7. Conclusions

In this study, we investigated the K-Mg isotopic compositions of the shallow-sea shelf sediments from the Bohai Sea, the Yellow Sea, the East China Sea, and Hainan island offshore. The samples span 22° in latitude (18°N to 40°N) and cover temperate, subtropical, and tropical monsoon climatic regimes. Our study demonstrates that K isotope ratios are sensitive to climate-related chemical weathering, and we first

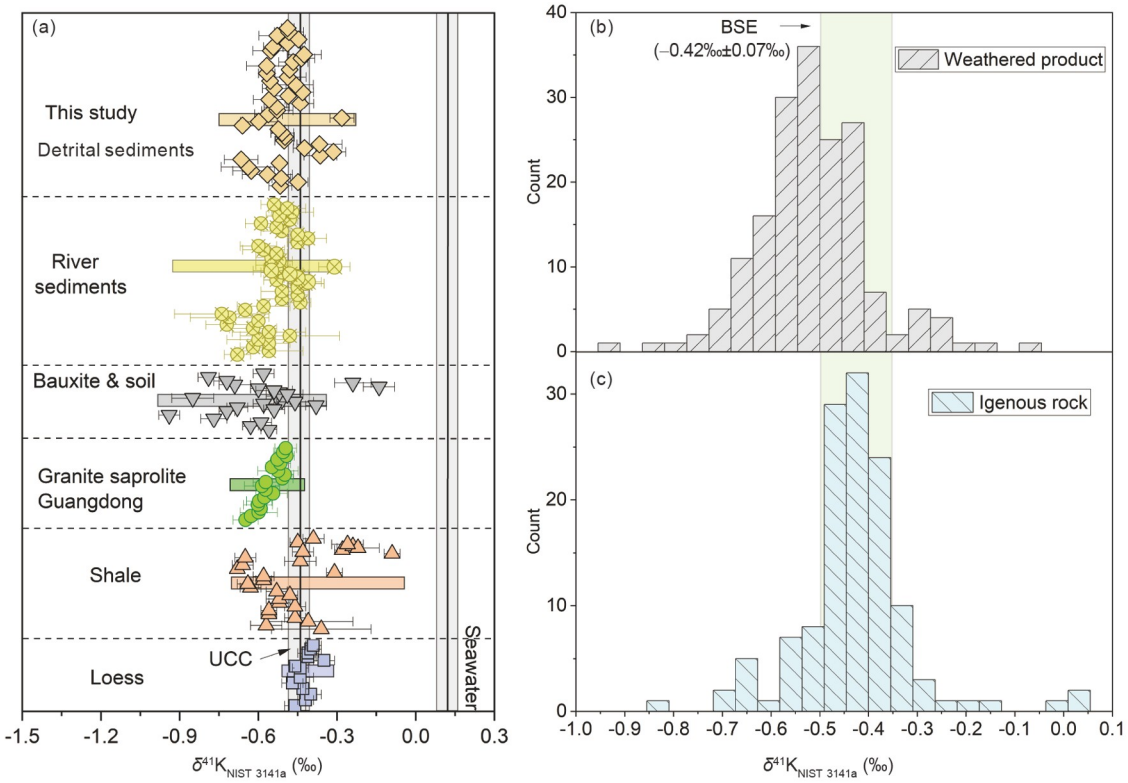

Figure 7 K isotopic composition of different geological reservoirs. (a) Statistical diagram of potassium isotopic variations of loess, shale, weathered profiles, river and shallow-sea shelf sediments; (b) histogram of compiled δ^{41}K data of the terrigenous weathered products, including loess, shale, soil, river sediments, residues in weathering profiles and shallow-sea shelf sediments; (c) histogram of compiled δ^{41}K data of igneous rocks. Data source of weathering products: this study and Morgan et al. (2018), Chen et al. (2019), Li W Q et al. (2019), Li S L et al. (2019), Li X Q et al. (2020,2022), Huang et al. (2020), Teng et al. (2020), Li W S et al. (2021a). Data source of igneous rocks: Chen et al. (2019), Tuller-Ross et al. (2019a, 2019b), Xu et al. (2019), Sun et al. (2020), Teng et al. (2020), Hu et al. (2021) and Wang Z Z et al. (2021).

reveal a potential link between the K isotope variability of detrital sediments and climatic conditions. This study also has important implications for paleoclimate reconstruction and K isotope heterogeneity of continental crust. The following concluding remarks are reached:

(1) Potassium isotope composition of detrital sediments could be used to study continental-scale chemical weathering.

(2) Physical perturbation due to the prevailing seasonal coastal currents and episodic events (i.e., storm, tidal wave, turbidity flows) can lead to relatively tight δ^{41}K values in detrital sediments. Considerable variation in δ^{41}K values and correlations with the chemical weathering indices are preserved in detrital sediments with less mixing and perturbations.

(3) The δ^{41}K values of the weathering residue show a broad decrease with increasing precipitation, implying that K isotopes of detrital sediments could be used to investigate paleoclimate and chemical weathering intensity.

Acknowledgements *We thank Yang ZHANG, Yifu FENG and Yang QU for the help in the samples' pretreatment; Chuan LIU for the assistance with Mg isotope analyses. The paper has been significantly improved by the two anonymous reviewers. This work was supported by the National Natural Science Foundation of China (Grant Nos. 92358301, 41873004).*

Conflict of interest The authors declare that they have no conflict of interest.

References

An S C, Luo X L, Li W Q. 2022. Precise measurement of ^{41}K/^{39}K ratios by high-resolution multicollector inductively coupled plasma mass spectrometry under a dry and hot plasma setting. Rapid Comm Mass Spectrometry, 36: e9289

Anderson S P. 2012. How deep and how steady is Earth's surface? Geology, 40: 863–864

Beaulieu E, Godderis Y, Labat D, Roelandt C, Oliva P, Guerrero B. 2010. Impact of atmospheric CO_2 levels on continental silicate weathering. Geochem Geophys Geosyst, 11: 1–8

Bian C W, Jiang W S, Song D H. 2010. Terrigenous transportation to the Okinawa Trough and the influence of typhoons on suspended sediment concentration. Cont Shelf Res, 30: 1189–1199

Brantley S L. 2008. Understanding soil time. Science, 321: 1454–1455

Chen C S, Lai Z G, Beardsley R C, Xu Q H, Lin H C, Viet N T. 2012. Current separation and upwelling over the southeast shelf of Vietnam in the South China Sea. J Geophys Res, 117: 2011JC007150

Chen F H, Xu Q H, Chen J H, Birks H J, Liu J B, Zhang S R, Jin L Y, An C B, Telford R J, Cao X Y, Wang Z L, Zhang X J, Selvaraj K, Lu H Y, Li Y C, Zheng Z, Wang H P, Zhou A F, Dong G H, Zhang J W, Huang X Z, Bloemendal J, Rao Z G. 2015. East Asian summer monsoon pre-

cipitation variability since the last deglaciation. Sci Rep, 5: 11186
Chen H, Liu X M, Wang K. 2020. Potassium isotope fractionation during chemical weathering of basalts. Earth Planet Sci Lett, 539: 116192
Chen H, Tian Z, Tuller-Ross B, Korotev R L, Wang K. 2019. High-precision potassium isotopic analysis by MC-ICP-MS: An inter-laboratory comparison and refined K atomic weight. J Anal At Spectrom, 34: 160–171
Chen J, Wu X D, Finlayson B L, Webber M, Wei T Y, Li M T, Chen Z Y. 2014. Variability and trend in the hydrology of the Yangtze River, China: Annual precipitation and runoff. J Hydrol, 513: 403–412
Chen X Y, Teng F Z, Huang K J, Algeo T J. 2020. Intensified chemical weathering during Early Triassic revealed by magnesium isotopes. Geochim Cosmochim Acta, 287: 263–276
Cheng H, Edwards R L, Sinha A, Spotl C, Yi L, Chen S T, Kelly M, Kathayat G, Wang X F, Li X L, Kong X G, Wang Y L, Ning Y F, Zhang H W. 2016. The Asian monsoon over the past 640,000 years and ice age terminations. Nature, 534: 640–646
Christensen J N, Qin L P, Brown S T, DePaolo D J. 2018. Potassium and calcium isotopic fractionation by plants (Soybean [*Glycine max*], Rice [*Oryza sativa*], and Wheat [*Triticum aestivum*]). ACS Earth Space Chem, 2: 745–752
Collins W J, Richards S W. 2008. Geodynamic significance of S-type granites in circum-Pacific orogens. Geology, 36: 559–562
Dellinger M, Gaillardet J, Bouchez J, Calmels D, Louvat P, Dosseto A, Gorge C, Alanoca L, Maurice L. 2015. Riverine Li isotope fractionation in the Amazon River basin controlled by the weathering regimes. Geochim Cosmochim Acta, 164: 71–93
Dessert C, Dupré B, François L M, Schott J, Gaillardet J, Chakrapani G, Bajpai S. 2001. Erosion of Deccan Traps determined by river geochemistry: Impact on the global climate and the $^{87}Sr/^{86}Sr$ ratio of seawater. Earth Planet Sci Lett, 188: 459–474
Dong J, Li A C, Liu X T, Wan S M, Xu F J, Shi X F. 2020. Holocene climate modulates mud supply, transport, and sedimentation on the East China sea shelf. J Geophys Res-Earth Surf, 125: e2020JF005731
Dunlea A G, Murray R W, Sauvage J, Spivack A J, Harris R N, D'Hondt S. 2015. Dust, volcanic ash, and the evolution of the South Pacific Gyre through the Cenozoic. Paleoceanography, 30: 1078–1099
Eberl D D. 1984. Clay mineral formation and transformation in rocks and soils. Phil Trans R Soc Lond A, 311: 241–257
Gaillardet J, Millot R, Dupré B. 2003. Chemical denudation rates of the western Canadian orogenic belt: The Stikine terrane. Chem Geol, 201: 257–279
Gao S, Wang D D, Yang Y, Zhou L, Zhao Y Y, Gao W H, Han Z C, Yu Q, Li G C. 2016. Holocene sedimentary systems on a broad continental shelf with abundant river input: Process-product relationships. Geol Soc Lond Spec Publ, 429: 223–259
Garcia D, Fonteilles M, Moutte J. 1994. Sedimentary fractionations between Al, Ti, and Zr and the genesis of strongly peraluminous granites. J Geol, 102: 411–422
Gong C L, Steel R J, Wang Y M, Lin C S, Olariu C. 2016. Shelf-margin architecture variability and its role in sediment-budget partitioning into deep-water areas. Earth-Sci Rev, 154: 72–101
Guan B X. 1994. Patterns and structures of the currents in Bohai, Huanghai and East China Seas. In: Zhou D, Liang Y B, Zeng C K, eds. Oceanology of China Seas. Dordrecht: Springer Netherlands. 17–26
Guo Y W, Yang S Y. 2016. Heavy metal enrichments in the Changjiang (Yangtze River) catchment and on the inner shelf of the East China Sea over the last 150 years. Sci Total Environ, 543: 105–115
Hayes N R, Buss H L, Moore O W, Krám P, Pancost R D. 2020. Controls on granitic weathering fronts in contrasting climates. Chem Geol, 535: 119450
Hopkinson T N, Harris N B W, Warren C J, Spencer C J, Roberts N M W, Horstwood M S A, Parrish R R, Eimf R R. 2017. The identification and significance of pure sediment-derived granites. Earth Planet Sci Lett, 467: 57–63
Hu B Q, Li J, Cui R Y, Wei H L, Zhao J T, Li G G, Fang X S, Ding X, Zou L, Bai F L. 2014. Clay mineralogy of the riverine sediments of Hainan Island, South China Sea: Implications for weathering and provenance. J Asian Earth Sci, 96: 84–92
Hu J Y, Wang X H. 2016. Progress on upwelling studies in the China seas. Rev Geophys, 54: 653–673
Hu Y, Teng F Z, Chauvel C. 2021. Potassium isotopic evidence for sedimentary input to the mantle source of Lesser Antilles lavas. Geochim Cosmochim Acta, 295: 98–111
Hu Y, Teng F Z, Plank T, Chauvel C. 2020. Potassium isotopic heterogeneity in subducting oceanic plates. Sci Adv, 6: eabb2472
Hu Y, Teng F Z, Plank T, Huang K J. 2017. Magnesium isotopic composition of subducting marine sediments. Chem Geol, 466: 15–31
Huang K J, Teng F Z, Elsenouy A, Li W Y, Bao Z Y. 2013. Magnesium isotopic variations in loess: Origins and implications. Earth Planet Sci Lett, 374: 60–70
Huang K J, Teng F Z, Wei G J, Ma J L, Bao Z Y. 2012. Adsorption- and desorption-controlled magnesium isotope fractionation during extreme weathering of basalt in Hainan Island, China. Earth Planet Sci Lett, 359–360: 73–83
Huang K J, Teng F Z, Shen B, Xiao S H, Lang X G, Ma H R, Fu Y, Peng Y B. 2016. Episode of intense chemical weathering during the termination of the 635 Ma Marinoan glaciation. Proc Natl Acad Sci USA, 113: 14904–14909
Huang T Y, Teng F Z, Rudnick R L, Chen X Y, Hu Y, Liu Y S, Wu F Y. 2020. Heterogeneous potassium isotopic composition of the upper continental crust. Geochim Cosmochim Acta, 278: 122–136
Kump L R, Brantley S L, Arthur M A. 2000. Chemical Weathering, Atmospheric CO_2, and Climate. Annu Rev Earth Planet Sci, 28: 611–667
Kurtz A C, Derry L A, Chadwick O A, Alfano M J. 2000. Refractory element mobility in volcanic soils. Geology, 28: 683–686
Kutzbach J E, Liu X D, Liu Z Y, Chen G S. 2008. Simulation of the evolutionary response of global summer monsoons to orbital forcing over the past 280,000 years. Clim Dyn, 30: 567–579
Li M, Xie L L, Zong X L, Li J Y, Li M M, Yan T, Han R L. 2022. Tidal currents in the coastal waters east of Hainan Island in winter. J Ocean Limnol, 40: 438–455
Li M Y H, Teng F Z, Zhou M F. 2021. Phyllosilicate controls on magnesium isotopic fractionation during weathering of granites: Implications for continental weathering and riverine system. Earth Planet Sci Lett, 553: 116613
Li S L, Li W Q, Beard B L, Raymo M E, Wang X M, Chen Y, Chen J. 2019. K isotopes as a tracer for continental weathering and geological K cycling. Proc Natl Acad Sci USA, 116: 8740–8745
Li W Q, Beard B L, Li S L. 2016. Precise measurement of stable potassium isotope ratios using a single focusing collision cell multi-collector ICP-MS. J Anal At Spectrom, 31: 1023–1029
Li W Q, Li S L, Beard B L. 2019. Geological cycling of potassium and the K isotopic response: Insights from loess and shales. Acta Geochim, 38: 508–516
Li W Q, Zhao S G, Wang X M, Li S L, Wang G G, Yang T, Jin Z D. 2020. Fingerprinting hydrothermal fluids in porphyry Cu deposits using K and Mg isotopes. Sci China Earth Sci, 63: 108–120
Li W S, Liu X M, Hu Y, Teng F Z, Hu Y F, Chadwick O A. 2021a. Potassium isotopic fractionation in a humid and an arid soil-plant system in Hawai'i. Geoderma, 400: 115219
Li W S, Liu X M, Wang K, Koefoed P. 2021b. Lithium and potassium isotope fractionation during silicate rock dissolution: An experimental approach. Chem Geol, 568: 120142
Li W S, Liu X M, Wang K, McManus J, Haley B A, Takahashi Y, Shakouri M, Hu Y. 2022a. Potassium isotope signatures in modern marine sediments: Insights into early diagenesis. Earth Planet Sci Lett, 599: 117849
Li W S, Liu X M, Wang K, Takahashi Y, Hu Y, Chadwick O A. 2022b. Soil potassium isotope composition during four million years of ecosystem development in Hawai'i. Geochim Cosmochim Acta, 332: 57–77
Li X Q, Han G L, Liu M, Liu J K, Zhang Q, Qu R. 2022. Potassium and its isotope behaviour during chemical weathering in a tropical catchment affected by evaporite dissolution. Geochim Cosmochim Acta, 316:

105–121
Li X Q, Han G L, Zhang Q, Miao Z. 2020. An optimal separation method for high-precision K isotope analysis by using MC-ICP-MS with a dummy bucket. J Anal At Spectrom, 35: 1330–1339
Liu C, Li W Q. 2020. Transformation of amorphous precursor to crystalline carbonate: Insights from Mg isotopes in the dolomite-analogue mineral norsethite [$BaMg(CO_3)_2$]. Geochim Cosmochim Acta, 272: 1–20
Liu H Y, Wang K, Sun W D, Xiao Y L, Xue Y Y, Tuller-Ross B. 2020. Extremely light K in subducted low-T altered oceanic crust: Implications for K recycling in subduction zone. Geochim Cosmochim Acta, 277: 206–223
Liu X M, Teng F Z, Rudnick R L, McDonough W F, Cummings M L. 2014. Massive magnesium depletion and isotope fractionation in weathered basalts. Geochim Cosmochim Acta, 135: 336–349
Liu X T, Li A C, Dong J, Lu J, Huang J, Wan S M. 2018. Provenance discrimination of sediments in the Zhejiang-Fujian mud belt, East China Sea: Implications for the development of the mud depocenter. J Asian Earth Sci, 151: 1–15
Lu J, Li A C, Zhang J, Huang P. 2019. Yangtze River-derived sediments in the southwestern South Yellow Sea: Provenance discrimination and seasonal transport mechanisms. J Asian Earth Sci, 176: 353–367
Ma F, Wang Y P, Li Y, Ye C J, Xu Z W, Zhang F. 2010. The application of geostatistics in grain size trend analysis: A case study of eastern Beibu Gulf. J Geogr Sci, 20: 77–90
Ma L, Teng F Z, Jin L X, Ke S, Yang W, Gu H O, Brantley S L. 2015. Magnesium isotope fractionation during shale weathering in the shale hills critical zone observatory: Accumulation of light Mg isotopes in soils by clay mineral transformation. Chem Geol, 397: 37–50
Mi B B, Zhang Y, Mei X. 2022. The sediment distribution characteristics and transport pattern in the eastern China seas. Quat Int, 629: 44–52
Morgan L E, Santiago Ramos D P, Davidheiser-Kroll B, Faithfull J, Lloyd N S, Ellam R M, Higgins J A. 2018. High-precision $^{41}K/^{39}K$ measurements by MC-ICP-MS indicate terrestrial variability of $\delta^{41}K$. J Anal At Spectrom, 33: 175–186
Moynier F, Vance D, Fujii T, Savage P. 2017. The isotope geochemistry of zinc and copper. Rev Mineral Geochem, 82: 543–600
Muhs D R, Bettis Iii E A, Been J, McGeehin J P. 2001. Impact of climate and parent material on chemical weathering in loess-derived soils of the Mississippi River Valley. Soil Sci Soc Amer J, 65: 1761–1777
Nesbitt H W, Young G M. 1982. Early Proterozoic climates and plate motions inferred from major element chemistry of lutites. Nature, 299: 715–717
Opfergelt S, Burton K W, Georg R B, West A J, Guicharnaud R A, Sigfusson B, Siebert C, Gislason S R, Halliday A N. 2014. Magnesium retention on the soil exchange complex controlling Mg isotope variations in soils, soil solutions and vegetation in volcanic soils, Iceland. Geochim Cosmochim Acta, 125: 110–130
Pang C G, Li K, Hu D X. 2016. Net accumulation of suspended sediment and its seasonal variability dominated by shelf circulation in the Yellow and East China Seas. Mar Geol, 371: 33–43
Parendo C A, Jacobsen S B, Kimura J I, Taylor R N. 2022a. Across-arc variations in K-isotope ratios in lavas of the Izu arc: Evidence for progressive depletion of the slab in K and similarly mobile elements. Earth Planet Sci Lett, 578: 117291
Parendo C A, Jacobsen S B, Plank T. 2022b. Potassium-isotope variations of marine sediments adjacent to the Izu-Bonin Trench and Nankai Trough. Geochim Cosmochim Acta, 337: 166–181
Parendo C A, Jacobsen S B, Wang K. 2017. K isotopes as a tracer of seafloor hydrothermal alteration. Proc Natl Acad Sci USA, 114: 1827–1831
Penman D E, Caves Rugenstein J K, Ibarra D E, Winnick M J. 2020. Silicate weathering as a feedback and forcing in Earth's climate and carbon cycle. Earth-Sci Rev, 209: 103298
Penniston-Dorland S, Liu X M, Rudnick R L. 2017. Lithium isotope geochemistry. Rev Mineral Geochem, 82: 165–217
Pogge von Strandmann P A E, Jenkyns H C, Woodfine R G. 2013. Lithium isotope evidence for enhanced weathering during oceanic anoxic event 2. Nat Geosci, 6: 668–672
Qiao S Q, Shi X F, Wang G Q, Zhou L, Hu B Q, Hu L M, Yang G, Liu Y G, Yao Z Q, Liu S F. 2017. Sediment accumulation and budget in the Bohai Sea, Yellow Sea and East China Sea. Mar Geol, 390: 270–281
Raymo M E, Ruddiman W F. 1992. Tectonic forcing of late cenozoic climate. Nature, 359: 117–122
Rudnick R, Gao S. 2014. Composition of the Continental Crust. In: Holland H D, Turekian K K, eds. Treatise on Geochemistry. 1–51
Santiago Ramos D P, Coogan L A, Murphy J G, Higgins J A. 2020. Low-temperature oceanic crust alteration and the isotopic budgets of potassium and magnesium in seawater. Earth Planet Sci Lett, 541: 116290
Santiago Ramos D P, Morgan L E, Lloyd N S, Higgins J A. 2018. Reverse weathering in marine sediments and the geochemical cycle of potassium in seawater: Insights from the K isotopic composition ($^{41}K/^{39}K$) of deep-sea pore-fluids. Geochim Cosmochim Acta, 236: 99–120
Shen B, Jacobsen B, Lee C T A, Yin Q Z, Morton D M. 2009. The Mg isotopic systematics of granitoids in continental arcs and implications for the role of chemical weathering in crust formation. Proc Natl Acad Sci USA, 106: 20652–20657
Sun H, Xiao Y L, Gao Y J, Zhang G J, Casey J F, Shen Y A. 2018. Rapid enhancement of chemical weathering recorded by extremely light seawater lithium isotopes at the Permian-Triassic boundary. Proc Natl Acad Sci USA, 115: 3782–3787
Sun Y, Teng F Z, Hu Y, Chen X Y, Pang K N. 2020. Tracing subducted oceanic slabs in the mantle by using potassium isotopes. Geochim Cosmochim Acta, 278: 353–360
Sweeney K E, Roering J J, Almond P, Reckling T. 2012. How steady are steady-state landscapes? Using visible-near-infrared soil spectroscopy to quantify erosional variability. Geology, 40: 807–810
Teng F Z. 2017. Magnesium isotope geochemistry. Rev Mineral Geochem, 82: 219–287
Teng F Z, Hu Y, Ma J L, Wei G J, Rudnick R L. 2020. Potassium isotope fractionation during continental weathering and implications for global K isotopic balance. Geochim Cosmochim Acta, 278: 261–271
Teng F Z, Li W Y, Rudnick R L, Gardner L R. 2010. Contrasting lithium and magnesium isotope fractionation during continental weathering. Earth Planet Sci Lett, 300: 63–71
Tuller-Ross B, Marty B, Chen H, Kelley K A, Lee H, Wang K. 2019a. Potassium isotope systematics of oceanic basalts. Geochim Cosmochim Acta, 259: 144–154
Tuller-Ross B, Savage P S, Chen H, Wang K. 2019b. Potassium isotope fractionation during magmatic differentiation of basalt to rhyolite. Chem Geol, 525: 37–45
Viers J, Dupré B, Gaillardet J. 2009. Chemical composition of suspended sediments in World Rivers: New insights from a new database. Sci Total Environ, 407: 853–868
von Blanckenburg F. 2006. The control mechanisms of erosion and weathering at basin scale from cosmogenic nuclides in river sediment. Earth Planet Sci Lett, 242: 224–239
Wang J Z, Li A C, Xu K H, Zheng X F, Huang J. 2015. Clay mineral and grain size studies of sediment provenances and paleoenvironment evolution in the middle Okinawa Trough since 17ka. Mar Geol, 366: 49–61
Wang K, Li W Q, Li S L, Tian Z, Koefoed P, Zheng X Y. 2021a. Geochemistry and cosmochemistry of potassium stable isotopes. Geochemistry, 81: 125786
Wang K, Peucker-Ehrenbrink B, Chen H, Lee H, Hasenmueller E A. 2021b. Dissolved potassium isotopic composition of major world rivers. Geochim Cosmochim Acta, 294: 145–159
Wang Z Z, Teng F Z, Prelević D, Liu S A, Zhao Z. 2021. Potassium isotope evidence for sediment recycling into the orogenic lithospheric mantle. Geochem Persp Let, 18: 43–47
Wei G Y, Chen T Y, Poulton S W, Lin Y B, He T C, Shi X F, Chen J F, Li H L, Qiao S Q, Liu J H, Li D, Ling H F. 2021. A chemical weathering control on the delivery of particulate iron to the continental shelf. Geochim Cosmochim Acta, 308: 204–216

Wei G Y, Wei W, Wang D, Li T, Yang X P, Shields G A, Zhang F F, Li G J, Chen T Y, Yang T, Ling H F. 2020. Enhanced chemical weathering triggered an expansion of euxinic seawater in the aftermath of the Sturtian glaciation. Earth Planet Sci Lett, 539: 116244

Xu J, Xia X P, Wang Q, Spencer C J, Lai C K, Ma J L, Zhang L, Cui Z X, Zhang W F, Zhang Y Q. 2021. Pure sediment-derived granites in a subduction zone. GSA Bull, 134: 599–615

Xu Y K, Hu Y, Chen X Y, Huang T Y, Sletten R S, Zhu D, Teng F Z. 2019. Potassium isotopic compositions of international geological reference materials. Chem Geol, 513: 101–107

Yu Y G, Wang H J, Shi X F, Ran X B, Cui T W, Qiao S Q, Liu Y G. 2013. New discharge regime of the Huanghe (Yellow River): Causes and implications. Cont Shelf Res, 69: 62–72

Zhang P, Pang Y, Pan H C, Shi C C, Huang Y W, Wang J J. 2015. Factors contributing to hypoxia in the Minjiang River Estuary, Southeast China. Int J Environ Res Public Health, 12: 9357–9374

Zhou X, Zhan T, Tu L Y, Smol J P, Jiang S W, Liu X Y, Xu C X, Guo Z T. 2022. Monthly insolation linked to the time-transgressive nature of the holocene East Asian monsoon precipitation maximum. Geology, 50: 331–335

(Editorial handling: Zhimin JIAN)